ELSEVIER

Journal of Power Sources 109 (2002) 313–320

JOURNAL OF POWER SOURCES

www.elsevier.com/locate/jpowsour

Thermal impedance spectroscopy for Li-ion batteries using heat-pulse response analysis

Evgenij Barsoukov*, Jee Hwan Jang, Hosull Lee

Kumho Chemical Laboratories, Korea Kumho Petrochemical Co. Ltd., P.O. Box 64, Yuseong, Taejeon 305-600, South Korea

Received 22 November 2001; accepted 7 February 2002

Abstract

Novel characterization of the thermal properties of batteries have been introduced by defining their frequency-dependent thermal impedance functions. The thermal impedance function can be approximated as a thermal impedance spectrum by analyzing the experimental temperature transient which is related to the thermal impedance function through Laplace transformation.

In order to obtain the temperature transient, a process has been devised to generate an external heat pulse with heating wire and to measure the response of the battery. This process is used to study several commercial Li-ion batteries of cylindrical type. Thermal impedance measurements have been performed using a potentiostat/galvanostat controlled by a digital signal processor, which is more commonly available than a flow-meter usually applied for thermal property measurements.

Thermal impedance spectra obtained for batteries produced by different manufacturers are found to differ considerably. Comparison of spectra at different states-of-charge indicates an independence of the thermal impedance on the charge state of the battery. It is shown that the thermal impedance spectrum can be used to obtain simultaneously the thermal capacity and the thermal conductivity of the battery by non-linear complex least-squares fit of the spectrum to the thermal impedance model.

Keywords: Thermal impedance spectrum; Thermal capacity; Thermal conductivity; Lithium-ion battery; Heat pulse

1. Introduction

As batteries have been principally employed in low-power applications, their thermal properties have not been relevant to the application design and therefore, have not been the subject of detailed research. This situation has changed markedly with the onset of new, high-power applications of batteries, such as portable computers, video-cameras, power-tools and hybrid electric vehicles. As the charge–discharge rates used in such devices can reach the 15 C rate (full discharge within 4 min), substantial heat development can occur in a short time. Thus, advanced heat management of batteries becomes important, particularly for large batteries or battery stacks, to prevent overheating damage or thermal runaway [1]. This is especially the care with Li-ion batteries which are capable of explosion and fire if overheated. The requirements of the engineering of high-power battery systems have resulted in increased attention being paid to the modeling of the thermal [2–4] and the combined electrochemical–thermal [5,6] behavior of batteries. For such modeling, it is necessary to know the experimental values of the thermal conductivity and the thermal capacity of each particular battery type. The thermal properties of many battery components have been studied by means of a guarded heat flow-meter used by Song et al. [7,8]. By way of example, theoretical calculations of the thermal conductivity and the capacity of an electrode stack of a Li-polymer battery are given in [4]. Such calculations are only possible if the composition of the battery stack is known exactly. Often, this information is available only to battery manufacturers. A further problem arises from the fact that the thermal characteristics of the stack components can change after exposure to electrolyte and the formation cycle. In situ measurements of these characteristics would give more precise information. Several recent papers have provided experimental data on the thermal capacity of the cells, measured by calorimetric technique [9,10]. By contrast, no in situ measured experimental data for the thermal conductivity of Li-ion batteries has been reported to date.

In this study, we present a new method to measure simultaneously both the thermal conductivity and the capacity of a battery which employs commonly available electrochemical equipment without the use of a calorimeter. The new method adopts the concept of the thermal impedance as a complete characteristic of a system's thermal properties.

* Corresponding author. Tel.: +82-42-865-8647; fax: +82-42-862-5661.
E-mail address: evgen@camd1.kkpcr.re.kr (E. Barsoukov).

0378-7753/02/$ – see front matter
PII: S0378-7753(02)00080-0

Such an approach has been employed before in different areas [11–13]. The method of measuring the thermal impedance using Laplace transformation of the temperature response transient to an external or an internal heat pulse is described in detail. To justify the new method experimentally, the thermal impedance spectra of cylindrical Li-ion batteries (18650 type) made by different manufacturers have been obtained. Especially, the dependence of thermal impedance on the state-of-charge is investigated for a Panasonic Li-ion battery. The specific thermal capacity and the conductivity are obtained for all batteries using a non-linear fit of the thermal impedance spectra to a model impedance function in the frequency-domain, developed for the case of cylindrical rod with interfacial heat development.

2. Derivation of thermal impedance functions

The thermal capacity and the thermal conductivity can be obtained by direct analysis of the temperature transient, which is measured after applying a heat pulse. Such analysis can be performed, for example, by fitting time-domain experimental data to a model function. Such a fit is often not practical where system is so complicated that its response cannot be described analytically and has to be calculated numerically using considerable computing resources. When some unaccounted thermal time-constants are present in the system, the fit to a beforehand-defined model function will not give indication about their presence or their nature. An alternative approach to analyze circuits with unknown structure is adapted in electronics. Representation of the transfer function of a circuit as a frequency-domain spectrum allows the parameters for all known elements of the circuit to be obtained while detecting all unexpected elements in case they are present.

The complex transfer function $F(s, x)$ defined in a Laplace-domain is commonly derived in an intermediate step for the temperature transient calculation by the Laplace method. If a small temperature change is expected transients can be derived as $T(t) = L^{-1}\{F(s,x)\}$, where L^{-1} is the inverse Laplace transform, s the complex frequency $2\pi f i + b$, f the frequency, i the imaginary multiplier, b the arbitrary real number, and x the space coordinate. Such functions have been derived for large variety of shapes of the heat conductors and heat application boundaries as solutions of *subsidiary equations* [14].

Exploiting the mathematical analogy between the formalisms which describe linear time-invariant electrical networks and thermal conductors, we can represent $F(s, x)$ as a product of two functions $I(s)$ and $Zt(s, x)$. Here, the first function is the Laplace transform of heat excitation and the second is a complete description of the thermal properties of the system which are dependent on the thermal conductivity, thermal capacity and shape of the thermal conductor.

When the function $Zt(s, x)$ is known, in a special case when $b = 0$ and space coordinate is fixed, $Zt(2\pi fi)$ is mathematically analogous to electrical impedance and is called here the 'thermal impedance function'. In contrast to time-domain response functions, thermal impedance functions have, in most cases, analytical expressions. These functions can be evaluated for a set of given frequencies f_1 as a set of complex numbers Zt_i which represents a thermal impedance spectrum. The thermal impedance spectrum can be visualized as an electrical impedance spectrum in a complex plot. The spectrum in such presentation gives indications about the contributions of different parts of the system to heat transfer and allows detection of the relative changes of thermal properties even by simple visual observation. Thermal resistance and thermal capacitance can be geometrically deduced from the spectrum in a complex plot. For example, the value of a serial resistor can be obtained from the highest frequency point of the spectrum, and the value of parallel resistors from the diameter of the semicircle.

Due to the mathematical similarity to the electrical model, thermal impedance functions can be derived similarly to electric impedance functions, essentially using the Ohm and Kirchhoff laws. In this approach, heat flow is treated as a current equivalent and temperature gradient as a voltage equivalent. Accordingly, the thermal resistance can be defined through the traditional specific thermal conductivity κ as $R_T = l/\kappa A$ (K s/J), and the thermal capacitance through the volume-specific heat $C_T = cAl$ (J/K). Here, A is the cross-section and l is the length of the elementary heat conduction region. By analogy with corresponding electric components, the complex impedance of these components are $Z(R_T) = R_T$ and $Z(C_T, s) = 1/C_T s$ where s is the complex frequency $2\pi fi$. Calculation of the complete thermal impedance function of a thermal conductor can be performed by setting up an "equivalent thermal circuit" and by applying the same rules as for electric elements to find the complete impedance between two desired points of the circuit.

Let us consider the case of a thin plate, with thickness l, specific heat c and exposed to air so that the thermal conductivity per unit surface due to radiation cooling is k, which is being internally heated. The temperature response is measured by a thermocouple on the surface. The thermal equivalent circuit will be a thermal resistor $R_{rc} = 1/\kappa A$ in parallel with a thermal capacitor $C_c = clA$. The thermal resistance of the thermocouple can be represented as a serial thermal resistance R_{ser}. Such a model gives a good description of thermal behavior of the battery casing and the heating coil. The thermal impedance of this model is given by:

$$Z(s) = \frac{1}{(1/R_{rc}) + C_c s} + R_{ser} \quad (1)$$

Treatment of the function in terms of thermal resistance and capacitance can be undertaken by impedance fitting software, of the type commonly used in electrochemistry, such as MEISP developed by the Korea Kumho Petrochemical Co. Ltd., then converting the obtained parameters into specific thermal values.

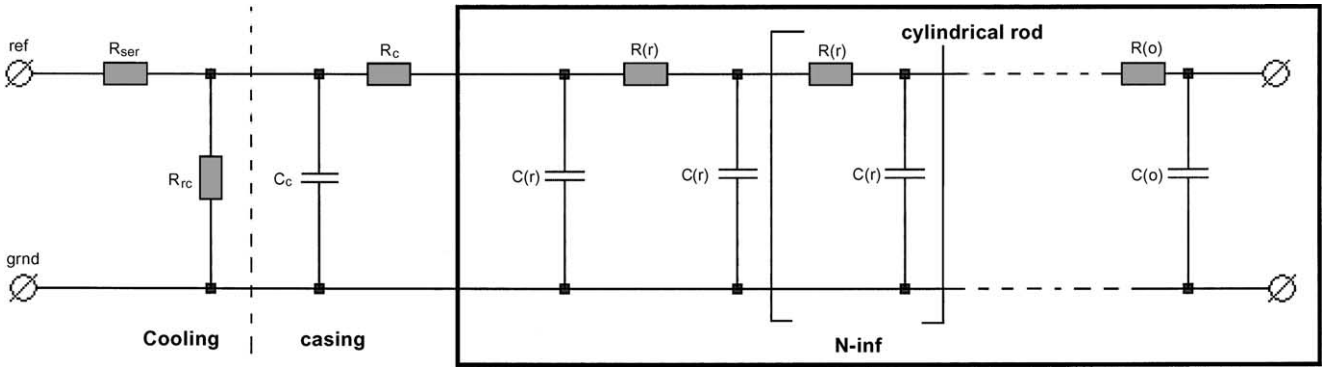

Fig. 1. Thermal equivalent circuit corresponding to cylindrical battery heated from surface under radiation cooling condition.

In many cases, an impedance function for an electric equivalent circuit is known and can be applied for the thermal conduction model. For example, the thermal equivalent circuit for a set-up, where a constant heat flow is applied to one side of a slab and another side is thermally insulated, is equivalent to an open-circuit terminated transmission line in electronics. Its impedance function is already known as:

$$Z(s) = \sqrt{\frac{R_T}{C_T s}} \coth\left(\sqrt{R_T C_T s}\right) \tag{2}$$

This equation (divided by a factor of two) expresses the thermal impedance of a prismatic battery to which a heat pulse is applied from the two opposite wide sides, and where the heat flow through its thin sides can be neglected.

The thermal model for a cylindrical battery, with heat excitation applied from the surface and with negligible heat flow over the sides, is analogous to a diffusion model developed for infinite cylindrical rod. Its impedance function has been derived as a solution of the *subsidiary equation* in [14] and as an electrochemical impedance for diffusion towards the center of the cylindrical rod in [15]:

$$Z(s) = \frac{I_0\left(\sqrt{2T_T C_T s}\right)}{\left(\sqrt{2R_T C_T s}\right) I_1\left(\sqrt{2R_T C_T s}\right)} R_T \tag{3}$$

and where I_0 and I_1 are Bessel functions of the first kind, with 0 and 1 order, respectively. Note that transformation from a cylindrical coordinate system to a Cartesian system is required to calculate specific thermal conductivity and capacity from the R and C obtained from the fit. The application of the transformation results in equations for specific thermal values, i.e.

$$k = \frac{1}{2\pi l R} \tag{4}$$

$$c = \frac{C}{\pi r^2 l} \tag{5}$$

where r is the radius of the battery and l the length.

In addition to a cylindrical thermal conductor which represents the bulk of a battery electrode stack, the thermal capacity of the battery casing together with the heating coil C_c and the thermal resistance between the casing and electrode stack R_c should be included in the thermal model. When the battery surface is exposed to air, heat flow through radiation and convection has to be considered. Using the thermal circuit approach, this is easily done by adding a 'thermal resistor' R_{rc} in parallel to the impedance in Eq. (3). It can be recalculated give the commonly used *heat transfer coefficient* h as $h = 1/(R_{rc} 2\pi r l)$.

Additionally, the thermal resistance between the surface and the thermocouple should be considered as a serial thermal resistance. The complete thermal equivalent circuit corresponding to a cylindrical Li-ion battery is shown in Fig. 1. The impedance function corresponding to the circuit is given in Eq. (6) as follows:

$$Z(s) = \left[\frac{1}{\left(I_0\left(\sqrt{2R_T C_T s}\right)/\left(\sqrt{2R_T C_T s}\right) I_1\left(\sqrt{2R_T C_T s}\right)\right) R_T + R_c} + \frac{1}{R_{rc}} + C_c s \right]^{-1} + R_{ser} \tag{6}$$

3. Measurement of thermal impedance spectrum

The thermal impedance function can be obtained directly from time-domain response to heat excitation without any presumption about internal structure of the circuit as given in Eq. (7):

$$Zt(s) = \frac{L\{T(t)\}}{L\{i(t)\}} \tag{7}$$

where $L\{\ \}$ denotes a Laplace transform, $T(t)$ is a temperature response function, and $i(t)$ is an excitation function in the time-domain. For example, if $i(t)$ is a heat pulse, it can be expressed as heat-flow amplitude I_0 (J/s) multiplied by a Heavisde step-function $\Phi(t)$ defined as 0 if $t < 0$ and 1 otherwise, $i(t) = I_0 \Phi(t)$. Its Laplace transform can be easily calculated as $L\{I_0 \Phi(t)\} = I_0/s$.

On the other hand, the analytical form of $T(t)$ is generally not known. Information about it is obtained from an experiment as a set of time-dependent samples T_i collected with time interval δt during sampling period Δt. The information about function $Zt(2\pi fi)$ is valid in a frequency range defined

by the sampling period and interval. Quantitatively the validity boundaries are given by the Nuquist theorem, $f_{max} = 1/2t$ and $f_{min} = 1/\Delta t$. A straightforward way to calculate the impedance spectrum based on such set of samples includes interpolation of the samples with piecewise-linear or other functions, followed by numerical integration of the resulting function to evaluate the transform integral in Eq. (8) for $s = 2\pi fi + b$ with frequency f ranging from f_{max} to f_{min}, while b is chosen so that the integral converges. Different methods to define b and resulting approximated solutions of the transform integral have been proposed in [16–18]:

$$F(s) = \int_0^\infty f(t)\, e^{-st}\, dt \tag{8}$$

Numerical integration and selection of optimal b can be avoided by using an analytical Laplace transform of a piecewise-linear function. All methods based on interpolation and direct use of Eq. (8) are, however, quite sensitive to noise which is commonly present when T_i are acquired in experiment, and gives unacceptable results at a usually attainable noise level, as shown in [19]. Alternatively, conversion can be accomplished by fitting the experimental data to a physically relevant function which has sufficient degrees of freedom to describe all possible system responses. The parameter obtained can be substituted into an analytical expression of the Laplace transform of such a function. Such procedure called *carrier function Laplace transform* (CFLT) is found in [19] to exhibit superior noise-rejection capability. CFLT is therefore used here to calculate $L\{T(t)\}$ which is then used to obtain the thermal impedance spectrum. The sum of an adaptively chosen number of exponents given in Eq. (9) is used as a carrier function in this case:

$$f(t) = \sum_{i=0}^{n} k_i\, e^{-(t/\tau_i)} \tag{9}$$

Laplace transform is as follows:

$$F(s) = \sum_{i=0}^{n} \frac{k_i}{(s + (1/\tau_i))} \tag{10}$$

Once the function parameters k_i and τ_i are obtained from a fit of the experimental temperature transient, the thermal impedance can be calculated combining Eq. (10) with Eq. (7), i.e.

$$Z(s) = \frac{s}{I} \sum_{i=0}^{n} \frac{k_i}{(s + (1/\tau_i))} \tag{11}$$

where I (W) is the magnitude of the heat flow applied to the surface of the heat conductor under test at time 0, and s is $2\pi fi$ where the frequency f can be selected between $1/\delta t$ and $1/\Delta t$.

4. Experimental set-up

To demonstrate the applicability of the proposed method in a real experimental environment and to obtain thermal impedance spectra for Li-ion batteries, we used our proprietary potentiostat/galvanostat with a digital signal processor (DSP) for signal generation and data acquisition. The system is known as the BPS 1000FL Powergraphy Battery Parameterization System.

Table 1
Characteristic parameters of batteries subjected to thermal impedance measurement

Manufacturer	Radius/ height (cm)	Weight (g)	Discharge capacity (mAh)
Moly Energy	0.9/6.5	42.72	1836
Panasonic	0.9/6.5	39.47	1536
Hitachi	0.9/6.5	41.57	1263
Samsung	0.9/6.5	40.93	1436

Cylindrical Li-ion batteries of the 18650 type with a specified capacity 1500 mAh and manufactured by Sony, Panasonic, LG and Samsung were obtained from commercial battery packs. Detailed characteristics of the batteries are given in Table 1.

In order to apply a constant heat flow to the surface of the batteries, a heating band made of Ni–Fe alloy with a total resistance of around 5 Ω and a negligible change in this value over the experimental temperature range were tightly wound around the battery, as shown in Fig. 2. A very thin contact wire was soldered on to the heating band to provide high electric conductivity but only very low stray thermal conductivity. The opposite ends of the contact wire were connected to the positive and the negative terminals of the BPS 1000FL, respectively. A thermocouple was fixed at the mid-point of the battery so that it touched the surface of battery but not the heating band. Readings from the thermocouple were performed by the BP1000FL and transmitted to the control PC. The battery was compressed between two plates of thermal insulator (porous polystyrene) in order to minimize heat conduction along the battery axis and through its sides. To increase the transfer of heat from the battery surface and, thereby, decrease the largest thermal

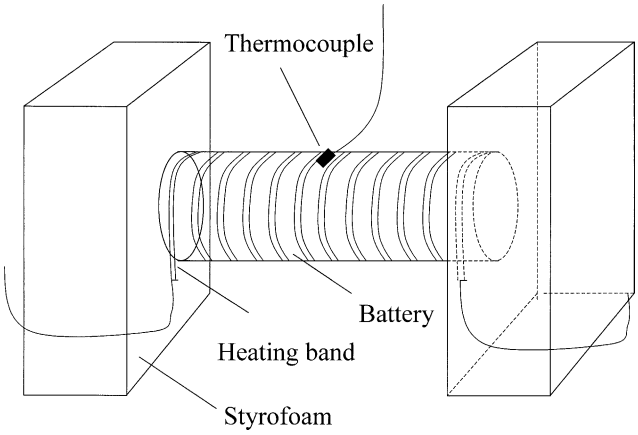

Fig. 2. Experimental set-up for thermal impedance measurement on cylindrical battery using external heating coil for generating heat pulse.

time-constant of the system, a 2 W CPU-cooler fan was placed 1 cm from the battery to provide convection cooling. Experiments were performed in an incubator at 20 °C with an average temperature fluctuation of 0.05 °C.

Before each measurement, the resistance of the coil was measured at a frequency of 1 kHz using the impedance measuring capabilities of the BPS 1000FL. With the exact value of resistance, the amount of current to apply a heat pulse of 1 W to the surface of the cell was calculated. The current was applied to the heating band with a rise time of 40 μs. The temperature response was measured with a sampling rate $\delta t = 20$ ms during period of $\Delta t = 1000$ s. Calculations of the impedance spectra were performed automatically by the BPS 1000FL control software using the algorithm described in Section 1. Parameters k_i were found by linear fit to eight exponents with time-constants t_i logarithmically selected between $f_{max} = 1/\delta t$ and $f_{min} = 1/\Delta t$. The fit was performed using the normal equation of the Gauss–Jordan elimination method [20].

5. Results and discussion

The thermal impedance of the heating coil used for the subsequent experiments was measured between 0.1 Hz and 1 mHz in order to obtain the specific heat capacity of the coil which will be used for correction of battery data. A heat pulse of 0.5 W was applied to the coil for 1000 s. The temperature transient data were converted to a thermal impedance spectrum as described. The resulting thermal impedance spectra together with the fit obtained using Eq. (1) are shown in Fig. 3. The MEISP non-linear least-squares fitting software developed by Kumho Petrochemical Co. Ltd. was used for analysis of the spectra. A good fit of the spectrum by the thermal impedance function indicates the correctness of the chosen thermal equivalent circuit model. The thermal capacity of the coil obtained by the fit is 4.12 J/K.

In order to separate the influence of the battery casing from the thermal behavior of the electrode stack, the thermal impedance spectrum of the empty casing was measured. The thermal capacity C_c of the casing together with the heating coil is found, by the fit of the spectrum, to be 13.74 J/K.

The thermal impedance spectrum of the Panasonic battery was measured over the wide frequency range of 0.1 Hz–100 μHz to check the validity of the proposed thermal model and to obtain the thermal capacity and the thermal conductivity of the battery. The resulting temperature transient is shown in Fig. 4 and the impedance spectrum together with the model fit is given in Fig. 5 as a complex plot. Two semicircles are visible on the plot. The depressed semicircle in the high-frequency part corresponds to the thermal capacity of the battery casing in parallel with thermal resistance between the casing and the electrode stack. The semicircle is depressed by the thermal resistance of the electrode stack. The low-frequency semicircle corresponds to the thermal capacity of the electrode stack in parallel with the thermal resistance of the interfacial cooling.

The parameters of the thermal model were obtained by fitting the spectrum to the thermal impedance function in Eq. (5). The casing capacity C_c obtained has been used as a fixed parameter in the fit. The good fit result indicates that the proposed thermal model satisfactorily describes the thermal behavior of the cylindrical Li-ion battery. All parameters resulting from the fit are listed in Table 2. As expected, thermal resistance of the thermocouple introduces a delay in the temperature onset and is therefore represented as a negative resistance in the thermal equivalent circuit. The

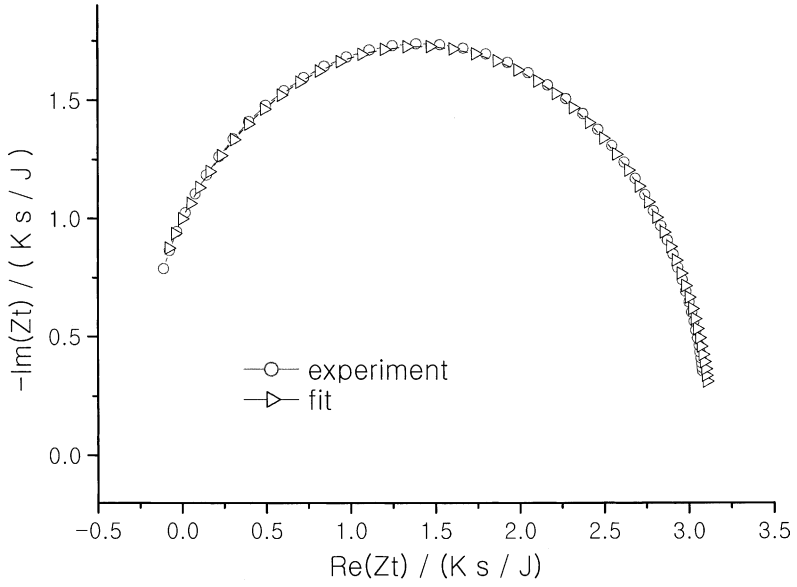

Fig. 3. Thermal impedance spectrum of heating coil, measured in frequency range 0.2 Hz–1 mHz. Fit line corresponds to the thermal impedance function for model described by Eq. (1).

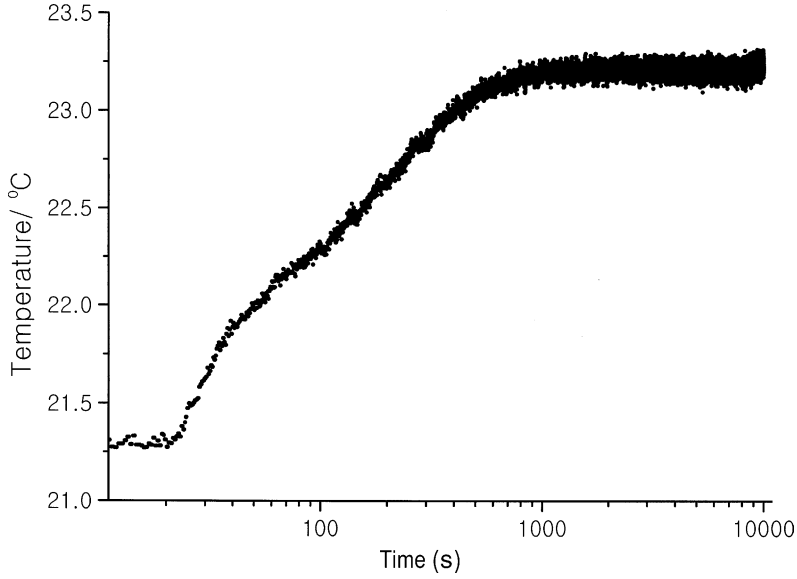

Fig. 4. Temperature transient in response to 1 W heat pulse applied to surface of Panasonic Li-ion battery.

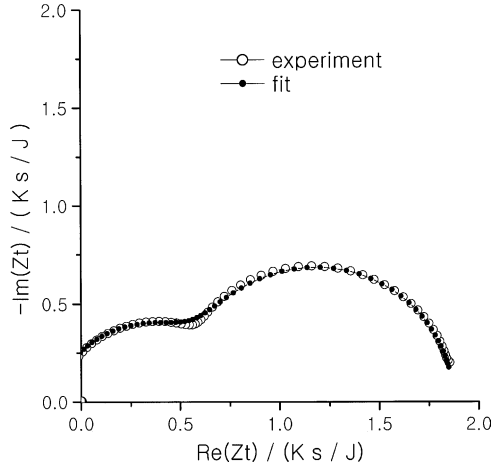

Fig. 5. Thermal impedance spectrum of Panasonic Li-ion battery in fully-charged state, measured between 0.1 Hz and 100 μHz. Fit line corresponds to the thermal model described by Eq. (5) with parameter values given in Table 2.

thermal capacity of the metal casing is found to be responsible for one-quarter of the total thermal capacity. A better thermal contact between the casing and the electrode stack can be important for improving the heat dissipation from battery, since the thermal resistance R_c between the casing and the stack is found to be one-third of the total thermal resistance of the battery. The thermal resistance at the battery surface due to radiation and convection cooling R_{rc} is the largest bottleneck in battery heat dissipation in spite of air circulation with a fan. Other contributions to total thermal impedance area, however, of the same order of magnitude. In the case of active cooling with water, as considered for high-power applications such as electric vehicles, the thermal resistance of the electrode stack can become dominant.

Specific values of the thermal parameters have been calculated using information about battery dimensions and weight in Table 1 and Eq. (4). To calculate the specific capacity of the casing, the thermal capacity of the coils subtracted, and a casing weight of 8.9 g was used. All specific values are given in Table 3. The specific thermal capacity of the electrode stack is 1.9 J/(K g) and is noticeably higher than that the battery previously reported as 1.07 J/(K g) in [9]. The thermal capacity of the casing is not considered separately in this paper. The thermal conductivity of the electrode stack perpendicular to the electrode surface is found to be 1.4 W/(K m), which is almost five times larger than that for a Li-polymer battery calculated in [4] on the basis of the known thermal conductivity of the component materials. This considerable difference probably

Table 2
Thermal equivalent circuit parameters obtained by fitting thermal impedance spectra of Li-ion batteries (Fig. 6) to thermal model in Fig. 1 described by Eq. (5)

Manufacturer	R_{ser} (K/W)	R_{rc} (K/W)	C_c (J/K)	R_c (K/W)	C_T (J/K)	R_T (K/W)
Moly Energy	−0.05	2.49	13.47	0	61.5	2.80
Panasonic	−0.1	1.98	13.74	0.90	58.4	1.78
Hitachi	−0.05	3.23	13.74	1.01	37.68	0.86
Samsung	−0.02	1.94	13.74	0	76.73	2.07

Table 3
Heat transfer coefficients, specific heat and thermal conductivity of cylindrical Li-ion batteries, obtained by fit of their thermal impedance spectra to thermal impedance function in Eq. (5) corresponding to thermal model given Fig. 1

Manufacturer	h_{rc} (W/(K m^2))	C_c (J/(K g))	h_c (W/(K m^2))	C_T (J/(K g))	κ_T (W/(K m))
Moly Energy	109.3	1.1	–	1.8	0.9
Panasonic	137.1	1.1	302.1	1.9	1.4
Hitachi	84.5	1.1	269.3	1.2	2.8
Samsung	140.2	1.1	–	2.4	1.2

Specific values are obtained using conversion equations given in Eq. (4).

arises, apart from the use of liquid electrolyte, from the fact that a wound electrode stack is used in commercial batteries (both cylindrical and prismatic) and not the parallel electrode arrangement adopted in the calculations. A wound electrode stack design results in a thermal conduction pathways in radial direction through highly thermally conductive current-collectors. The presence of such unaccounted thermal pathways can explain a much higher average thermal conductivity, as found in experiment. The value obtained for the transfer coefficient, viz. 137 W/(K m^2) is rather high compared with 25 W/(K m^2) which is usually assumed for radiation and active convection cooling [4]. This is probably due to the close placement of the fan to the surface.

Thermal impedance spectra were measured on fully-charged Li-ion batteries manufactured by Panasonic, Hitachi, Moly Energy and Samsung in frequency range 0.1 Hz–1 mHz. The results are given in Fig. 6. It can be seen that the spectra are distinctly different, in spite of the similar chemistry of the batteries. This observation highlights the importance of considering thermal properties, characteristic to each particular manufacturing technology, in designing heat management of large battery packs with high-power capabilities.

The obtained part of the low-frequency semicircle was sufficient to determine the thermal capacity of the tested batteries. In order to determine the thermal parameters, the spectra have been fitted to the thermal impedance function in Eq. (5). The resulting values of the thermal equivalent circuit elements are given in Table 2 and specific values are in listed Table 3.

An interesting difference is observed for Moly and Samsung batteries compared with Panasonic and Hitachi batteries. The latter two batteries have noticeable thermal resistance R_c between the casing and the electrode stack, while in the case of first two batteries this resistance is negligible. Absence of close mechanical contact between the electrode stack and the casing could be reasons for this additional thermal resistance. Such loose contact should obviously be avoided to improve the protection from battery overheating. The lowest specific thermal capacitance is observed for the Hitachi battery, which also has the lowest electric capacity as shown in Table 1. The increase of

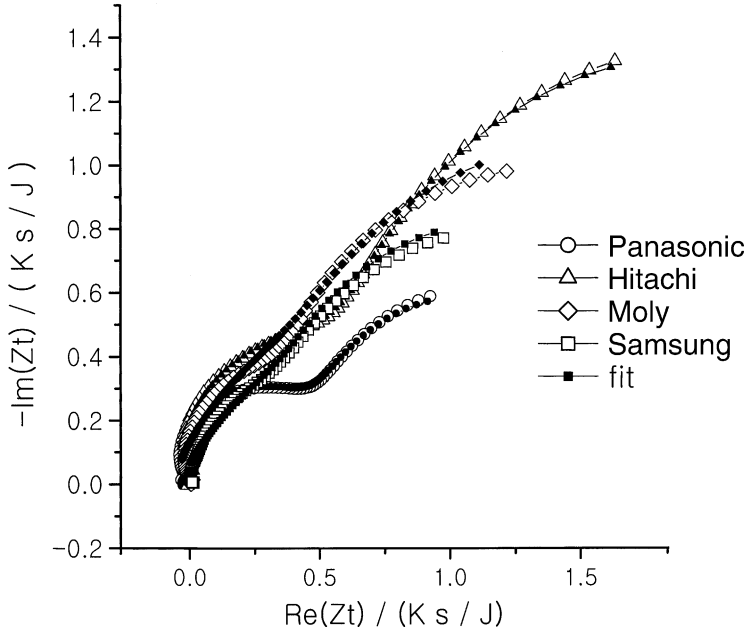

Fig. 6. Comparison of thermal impedance spectra of Panasonic, Moly Energy, Hitachi and Samsung Li-ion batteries measured between 0.1 Hz and 1 mHz. Fit lines correspond to thermal model described by Eq. (5) with parameter values given in Table 2.

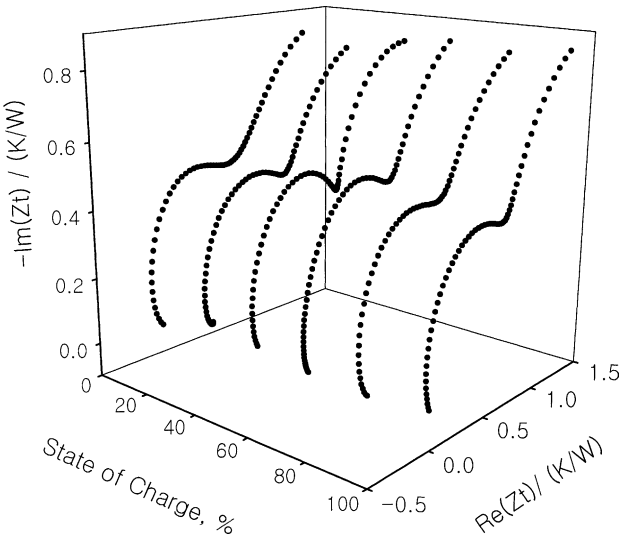

Fig. 7. Three-dimensional plot representing dependence of thermal impedance spectra of Panasonic battery on state-of-charge. Impedance spectra are obtained in frequency range from 0.1 Hz to 1 mHz. State-of-charge ranges from discharged state (0%) to fully-charged state (100%).

electric capacity in battery design is probably related to adding more components with high thermal capacity. The electrode stack of the Hitachi battery also has the highest thermal conductivity among all measured batteries. These two properties could be due to a relatively larger contribution of electrolyte to the total weight of battery.

In order to determine how sensitive thermal properties of a Li-ion battery are with respect to the state-of-charge, thermal impedance spectra of Panasonic Li-ion battery were obtained at different states-of-charge. The battery was fully charged and then subjected to a repetitive sequence of discharge at the 5 h rate for 1 h, relaxation for 30 min and impedance spectrum measurement until it was fully discharged. The impedance spectra obtained at different states of charge is shown in Fig. 7. It can be seen that the thermal properties of Li-ion battery are practically independent of the state-of-charge. The slight increase of the size of the semicircle in the high-frequency region with increasing state-of-charge indicates a reduction in the average thermal conductivity of the electrode stack. The thermal capacitance of the battery remains unchanged during discharge, as can be seen from the unchanged semicircle in the low-frequency region of the thermal impedance plot.

6. Conclusions

In this work, we have demonstrated a possibility of simultaneous measurement of thermal capacity and thermal conductivity of cylindrical batteries by analysis of a thermal pulse response. Derivation of the thermal impedance spectrum from the temperature response transient by carrier function Laplace transform has been described. Thermal impedance measurements have been performed on Li-ion batteries produced by Panasonic, Moly Energy, Hitachi and Samsung. Considerable differences in the thermal properties are observed despite the similar basic chemistry and design of the batteries.

The frequency-domain thermal impedance function for a cylindrical battery have been derived and applied to the analysis of thermal impedance spectra. Specific thermal conductivities and capacities have been calculated for all measured batteries by fitting experimental thermal impedance spectra to the theoretical function. These values can be used further in thermal modeling of batteries, which is applied for design of high-power systems such as electric vehicles. A large thermal resistance between the casing and the electrode stack detected for the Panasonic and Hitachi batteries. This indicates that closer fitting of the electrode stack can improve the high-power capabilities of these batteries.

The dependence of the thermal properties on the state-of-charge has been studied for a Panasonic Li-ion battery. It is found that thermal impedance spectrum is virtually unchanged during battery discharge. A slight increase in thermal conductivity with state-of-charge is observed.

References

[1] T. Miyamoto, in: Proceedings of the 13th International Electric Vehicle Symposium, October 13–16 (1996) Osaka, Japan, Vol. 1, 1996, p. 37.
[2] C.R. Pal, J. Newman, J. Electrochem. Soc. 142 (1995) 3274.
[3] M. Verbrugge, AIChE J. 41 (1995) 1550.
[4] L. Song, J.W. Evans, J. Electrochem. Soc. 147 (2000) 2087.
[5] Y. Chen, J.W. Evans, J. Electrochem. Soc. 140 (1993) 1833.
[6] C.R. Pal, J. Newman, J. Electrochem. Soc. 142 (1995) 3282.
[7] L. Song, Y. Chen, J.W. Evans, J. Electrochem. Soc. 144 (11) (1997) 3797.
[8] L. Song, J.W. Evans, J. Electrochem. Soc. 146 (3) (1999) 869.
[9] J.S. Hong, H. Maleki, S. Al Hallaj, L. Redey, J.R. Selman, J. Electrochem. Soc. 145 (1998) 1489.
[10] S. Al Hallaj, J. Prakash, J.R. Selman, J. Power Sources 87 (2000) 186.
[11] M. Carmona, S. Marco, J. Palacin, J. Samitier, IEEE Trans. Comput. Pack. Tech. 22 (2) (1999) 238.
[12] E. Delacre, D. Defer, B. Duthoit, ASME 1 (2000) 414.
[13] J.S. Turner, J. Therm. Biol. 19 (1994) 237.
[14] H.S. Carslaw, J.C. Jaeger, Conduction of Heat in Solids, 2nd Edition, Oxford University Press, Oxford, 1959.
[15] T. Jacobsen, K. West, Electrochim. Acta 40 (2) (1995) 255.
[16] A.A. Pilla, J. Electrochem. Soc. 117 (1970) 467.
[17] C.W. Meyers, J.K. Doughty, Raytheon Company, US Patent 5794008 (1996).
[18] J. Ye, K. Doblhofer, J. Electroanal. Chem. 272 (1989) 29.
[19] E. Barsoukov, J.H. Jang, H. Lee, Electrochem. Acta, submitted for publication.
[20] W.H. Press, S.A. Teukolsky, W.T. Vetterlin, B.P. Flannery, Numerical Recipes in Fortran, 2nd Edition, Cambridge University Press, Cambridge, 1992 (Chapter 15.4).